Biomicrofluidics ARTICLE scitation.org/journal/bmf

A cell lines derived microfluidic liver model for investigation of hepatotoxicity induced by drug-drug interaction

Cite as: Biomicrofluidics 13, 024101 (2019); doi: 10.1063/1.5070088
Submitted: 19 October 2018 · Accepted: 28 February 2019 ·
Published Online: 7 March 2019

Jiu Deng,[1,a)] Xiuli Zhang,[2,b),a)] Zongzheng Chen,[3,a)] Yong Luo,[1,b)] Yao Lu,[4] Tingjiao Liu,[5] Zhengzhi Wu,[3] Yu Jin,[3] Weijie Zhao,[1] and Bingcheng Lin[1,4,b)]

AFFILIATIONS

[1]State Key Laboratory of Fine Chemicals, Department of Chemical Engineering & School of Pharmaceutical Science and Technology, Dalian University of Technology, Dalian 116024, China
[2]College of Pharmaceutical Science, Soochow University, Soochow 215123, China
[3]The First Affiliated Hospital of Shenzhen University, Shenzhen Second People's Hospital, Shenzhen 518035, China
[4]Biotechnologhy Division, Dalian Institute of Chemical Physics, Chinese Academy of Sciences, Dalian 116011, China
[5]College of Stomatology, Dalian Medical University, Dalian 116044, China

[a)]**Contributions:** J. Deng, X. Zhang, and Z. Chen contributed equally to this work.
[b)]**Authors to whom correspondence should be addressed:** yluo@dlut.edu.cn; zhangxiuli@dicp.ac.cn; and bclin@dicp.ac.cn

ABSTRACT

The poor metabolic ability of cell lines fails to meet the requirements of an *in vitro* model for drug interaction testing which is crucial for the development or clinical application of drugs. Herein, we describe a liver sinusoid-on-a-chip device composed of four kinds of transformed cell lines (HepG2 cells, LX-2 cells, EAhy926 cells, and U937 cells) that were ordered in a physiological distribution with artificial liver blood flow and biliary efflux flowing in the opposite direction. This microfluidic device applied three-dimensional culturing of HepG2 cells with high density (10^7 ml^{-1}), forming a tightly connected monolayer of EAhy926 cells and achieving the active transport of drugs in HepG2 cells. Results showed that the device maintained synthetic and secretory functions, preserved cytochrome P450 1A1/2 and uridine diphosphate glucuronyltransferase enzymatic activities, as well as sensitivity of drug metabolism. The cell lines derived device enables the investigation of a drug-drug interaction study. We used it to test the hepatotoxicity of acetaminophen and the following combinations: "acetaminophen + rifampicin," "acetaminophen + omeprazole," and "acetaminophen + ciprofloxacin." The variations in hepatotoxicity of the combinations compared to acetaminophen alone, which is not found in a 96-well plate model, in the device were −17.15%, 14.88%, and −19.74%. In addition, this result was similar to the one tested by the classical primary hepatocyte plate model (−13.22%, 13.51%, and −15.81%). Thus, this cell lines derived liver model provides an alternative to investigate drug hepatotoxicity, drug-drug interaction.

INTRODUCTION

The liver is an important organ responsible for xenobiotic metabolism, detoxification, and immunoregulation and is a major target for drug and chemical-induced toxicity. Historically, liver toxicity is the most frequent safety issue ending clinical trials and can even cause the postmarket withdrawal of drug candidates resulting in a considerable loss of human and financial resources.[1] Later, it was found that the co-use of a supplementary drug sometimes can substantially reduce or enhance the hepatotoxicity of original drugs.[2] Screening of this kind of supplementary drug thus becomes important for new drug development as well as pharmaceutics.

In vitro models, such as a recombinant enzyme,[3,4] liver microsome,[5] and primary hepatocytes (HCs),[6] have a major role in evaluating the hepatotoxicity of the drug-drug combination. Specifically, primary hepatocytes are widely used at the preclinical stage because of their considerable metabolic ability. However, primary hepatocytes are not perfect, not only because the extraction of primary cells is experimentally cumbersome but also because of the limited

source of cells from a single donor, donor to donor variation, and de-differentiation that make the reproducibility of primary hepatocytes questionable. Immortal liver cell lines can address these issues; however, their poor metabolic ability limited their use in the hepatotoxicity assessment.[7] Thus, it can be assumed that if we can elevate the metabolic ability of immortal liver cell lines, they may be applied to hepatotoxicity assessment, thus providing an alternative platform to assess hepatotoxicity of the drug-drug combination. Recently, several studies reported that applying new strategies, such as three-dimensional (3D) culturing, co-culturing with surrounding cells, introducing fluid flow, and patterning cells in an ordered spatial arrangement, which create a physiologically biomimetic microenvironment, can improve the function of the original cells *in vitro*. For example, hepatocytes co-cultured with endothelial cells and fibroblasts have proven to promote liver-specific functions.[8] Besides, co-culturing other cells with stem cells not only provides a target cell source with multipotent differentiation capacity but also promotes tissue homeostasis, metabolism, growth, repair, and so on.[9] The essential mechanism of this phenomenon is that the microenvironment affects the phenotypes of cells.

Organ-on-a-chip is the cutting-edge technology to manage microenvironments of cells.[10–12] Recently, organ-on-chip for modelling the kidney,[13] lung,[14] brain,[15] heart,[16] and skin[17] has been successfully built to replicate organ-level functions. Meantime, many liver-on-chip devices have also been constructed to study liver biology and function, drug-induced liver injury or liver diseases.[18,19] For example, Rennert *et al.* inoculated four types of hepatic cells on both sides of a porous membrane and applied perfusion culture conditions to create a biomimetic liver model that is physiologically imitative.[20] The results showed that the presence of shear forces and the ordered spatial arrangement of the cells gave the model more realistic morphological and functional characteristics. Moreover, a vascularized human liver acinus microphysiological system was designed for modeling diseases and absorption, distribution, metabolism, excretion, and toxicity (ADME/T) testing, which create a vascular channel to recapitulate the 3D structure of the liver acinus.[21] Collectively, 3D co-culture of HCs with nonparenchymal cells [liver sinusoidal endothelial cells (LSECs), Kupffer cells (KCs), or hepatic stellate cells (HSCs)] was widely applied for maintaining HC morphology and function,[8,22] enhancing albumin and urea secretion,[23–26] and promoting cytochrome activity,[3,27] making it more accurate to detect drug-induced hepatotoxicity. Moreover, fluid flow is another key factor required to mimic physiological environments in the sinusoid, which influences the transport of drugs in the liver by inducing HC polarization and also by supporting long-term cultivation or yielding null effects.[23,28] However, the active transport of drugs in HCs—entered from the blood and discharged to the bile duct—is also essential for *in vitro* hepatotoxicity testing.

In this paper, we established a 3D liver-sinusoid-on-a-chip (LSOC), which incorporates four kinds of immortal cell lines (HepG2 cells, LX-2 cells, EAhy926 cells, and U937 cells), artificial liver blood flow, and artificial bile flow, to explore the hepatotoxicity caused by drug interactions. This liver chip, as well as the traditional primary hepatocyte plate model, was used to test the hepatotoxicity of acetaminophen-based drug-drug interactions. We measured the hepatotoxicity of acetaminophen and calculated the variation in hepatotoxicity of acetaminophen when a supplementary drug was applied. We compared the variation obtained from the LSOC device and primary hepatocyte plate model and found that the variation of hepatotoxicity of acetaminophen tested by the LSOC device was similar to that by primary hepatocytes on the plate. Thus, this immortal cell lines derived 3D LSOC device may be used as an alternative platform for the investigation of hepatotoxicity induced by drug-drug interactions.

MATERIALS AND METHODS

Cell culture

Cell lines

Human hepatocellular carcinoma HepG2 cells (ATCC® HB-8065TM) were cultured in DMEM-HG (Hyclone) medium supplemented with 10% FBS (Gibco™), 1% non-essential amino acids (NEAA; Gibco), 100 U ml^{-1} penicillin, 100 μg ml^{-1} streptomycin, human umbilical vein EAhy926 cells (obtained from Prof. Du, Institute of Process Engineering, Beijing), human stellate LX-2 cells (EMD Millipore, Billerica, MA, USA), and human histiocytic lymphoma (human monocyte) U937 cells (CRL-1593.2TM, ATCC) were cultured in DME/F-12 1:1 (1×) containing 10% FBS (Gibco), 100 U ml^{-1} penicillin, and 100 μg ml^{-1} streptomycin to mimic the functions of LSECs, HSCs, and KCs, respectively. All cells were cultured in a cell incubator with 5% CO_2 at 37 °C. When cell confluence reached 75%-90%, cells were subcultured after trypsin digestion, except for U937 cells that cultured in suspension and centrifuged every 2 days for subculture.

Primary cells

Primary rat hepatocytes were isolated from male SD rats (weighing 160-180 g) using a two-step liver digest perfusion,[29] and cultured in Williams E medium, supplemented with 10% fetal bovine serum (FBS) (Gibco), 2 mM GlutaMAX (Life Technologies), 100 U ml^{-1} penicillin, and 100 μg ml^{-1} streptomycin (Sigma-Aldrich). The methods of primary cells were carried out in accordance with the law of the Chinese Government and regulations of the State Project for Essential Drug Research and Development, China.

Fabrication and assembly sequence of chips

The fabrication of microfluidic devices was performed according to the standard soft lithography and microfabrication methods using SU8-3035 negative photoresist (Microchem Corp., Newton, CA, USA) and polydimethylsiloxane (PDMS, Sylgard 184, Dow Corning, USA). The entire chip contains two polymethyl methacrylate (PMMA) frames, three PDMS spacers, and two porous polycarbonate (PC) membranes (Whatman) with 1-μm pore size. Prior to assembly, EAhy926 cells were seeded on a trimmed porous PC membrane. After incubation for 1 day, LX-2 cells were seeded on the other side of the membrane. During this time, U937 cells were exposed to 50 ng ml^{-1} PMA (phorbol 12-myristate 13-acetate, Sigma-Aldrich) for 48 h to differentiate into functional macrophages.[30,31] After digestion, HepG2 cells were resuspended in the 12 mg ml^{-1} ice-cold basement membrane extractant (BME) (R&D Systems, McKinley Place, MN, USA) at 10^7 cells per ml immediately. Subsequently, the cell-seeded porous membrane and another blank membrane were

assembled with the three pre-sterilized PDMS spacers layer by layer. Concurrently, 20 μl of the cell/BME mixture was added to the middle chamber formed between the two porous membranes. Finally, the top and bottom PMMA substrates and the assembled PDMS chips were assembled at a final size of 4 × 2.5 cm by screws [Fig. 1(c)]. U937 cells were injected into the top chamber of the chip via a syringe. After standing for 2 h, pipes and a multi-channel peristaltic pump (205 S/CA12, Watson Marlow, UK) were connected to both top and bottom channels to provide perfusion condition at a rate of 1 μl min^{-1}. The main flowing zones of both top and bottom channels were equally sized with H × W × L = 150 μm × 1.5 mm × 15 mm.

Detection of urea and albumin

The amount of albumin and urea secreted into the "artificial blood" was measured every 24 h. Generally, the chip was perfused

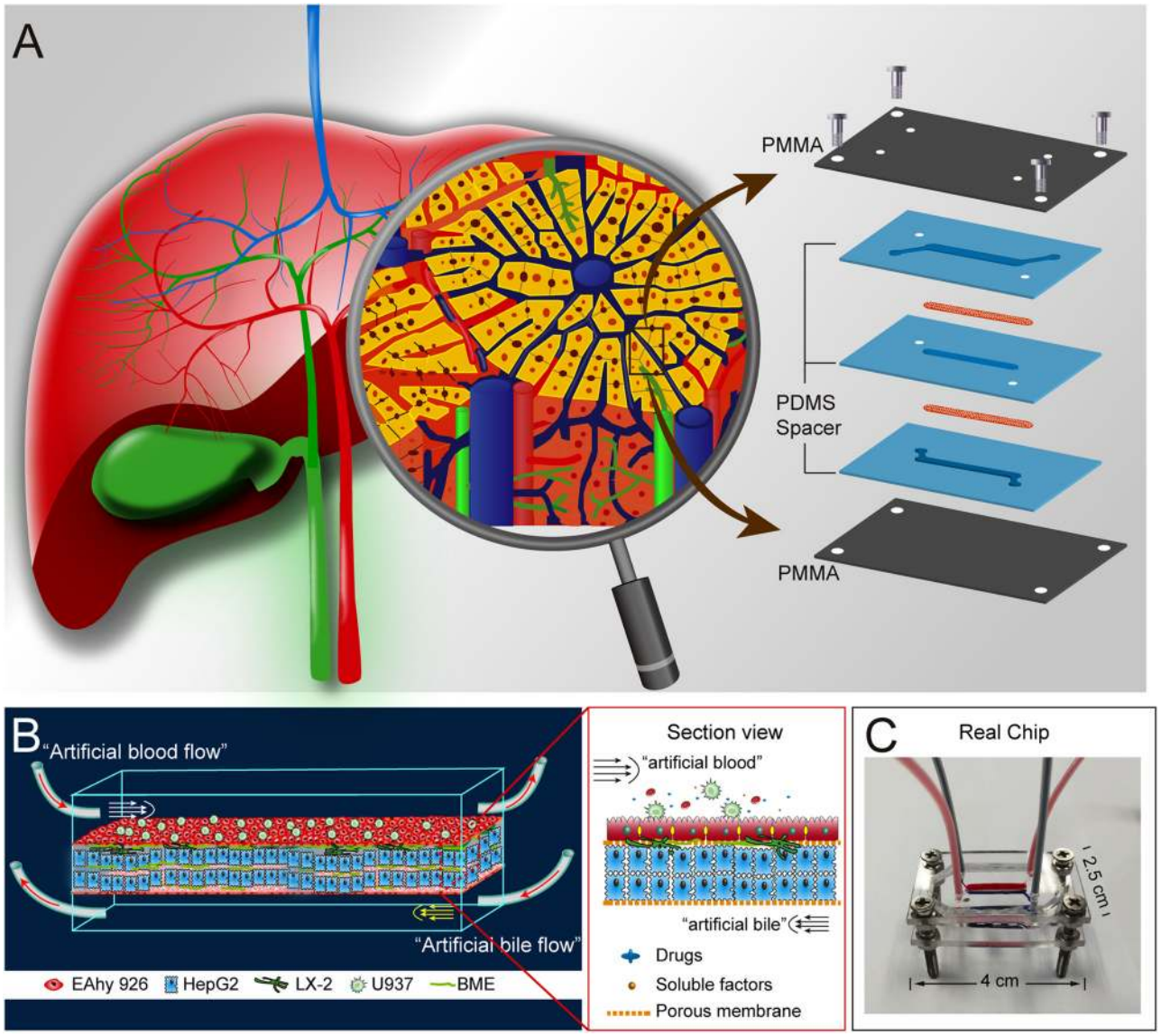

FIG. 1. Schematic of liver sinusoid structure and the LSOC microdevice. (a) Left: The illustration of the physiological structure of liver sinusoid in the liver. The liver sinusoid consists of four major types of hepatic cells—the liver hepatocytes, hepatic stellate cells, Kupffer cells, and sinusoidal endothelial cells—reside inside liver sinusoids and interact with flowing peripheral cells under blood flow. Right: The design of the LSOC microdevice. It consists of two layers of the PMMA substrate and three pieces of the PDMS spacer, which was divided by two pieces of cell seeded porous membrane to mimic the microenvironment of the liver sinusoid and its complex multiple cell-cell interactions *in vitro*. (b) Schematic diagram of 4 kinds of cell lines seeded in the device. (c) The real picture and size measurement of the chip.

with "artificial blood" [DMEM-HG (Hyclone) medium supplemented with 10% FBS (Gibco), 1% non-essential amino acids (NEAA; Gibco), 100 U ml^{-1} penicillin, 100 μg ml^{-1} streptomycin] and "artificial bile" ("artificial blood" without 10% FBS) for 24 h. The daily "artificial blood" in the top channel was collected and stored in a freezer at −80 °C before detection. The urea concentration in the medium was quantified by diacetylmonoxime [Blood Urea Nitrogen Stanbio Labs, Boerne, TX] using the colorimetric end point method. The amount of albumin was detected using the bromocresol green assay method according to the manual. The experimental results of albumin and urea were calculated by comparison with standard curves (Fig. S1 in the supplementary material), and the unit was converted to ng/day/10 000 cells (for details see the supplementary material: MTT assays and standard curves for cell number counting).

Detection of the activity of CYP 1A1/2 and glucuronidation

The activity of cytochrome P450 1A1/2 (CYP-1A1/2) was expressed by measuring the amount of resorufin, the fluorescent product of O-dealkylation of substrate 7-ethoxyresorcinin (7-ER, 7-ethoxyresorufin). Uridine diphosphate glucuronyltransferase (UGT) activity was expressed by detecting the content of 4-methylumbelliferone (4-MU) metabolite, 4-methylumbelliferyl glucuronide (4-MUG), in "artificial blood." Generally, for CYP 1A1/2 activity testing, 2.5 μM 7-ER and 10 μM dicumarol were added into "artificial blood" for incubating for 2 h, then the "artificial blood" was collected and fluorescence intensity was measured at 531/595 nm (ex/em) using a microplate reader (H1MF9, Genentech, USA). For UGT activity testing, 100 μM 4-MU was added into "artificial blood" for incubating for 5 h, then the fluorescence intensity of "artificial blood" was measured at 355/460 nm (ex/em) using a microplate reader. For the test without shear flow, the culture medium was exchanged every day and collected for measurement. For drug induction and inhibition experiments, models were pre-incubated with 50 μM omeprazole (OME), 25 μM ciprofloxacin (CPFX), 50 μM rifampicin (RIF), or 150 μM probenecid (PBD) as inducers or inhibitors of CYP 1A1/2 and UGT, respectively, for 48 h before activity assays followed by exposure to 7-ER + dicumarol or 4-MUG.

Polarization of HepG2 and visualization of bile canaliculus

The bile canaliculi were observed by carboxyfluorescein (CF). The chips were perfused for 3 h with "artificial blood" containing 2 μg ml^{-1} 5-(and-6)-carboxy-2′,7′-dichlorofluorescein diacetate (CDFDA) before being carefully disassembled. 3D HepG2 cells/BME mixture were obtained and washed three times in PBS, and then cultured for 1 h in complete medium and imaged under a fluorescence microscope. For quantitative analysis of active transportation of HepG2 cells in the device, the complete models [HepG2 (+) group] and models without HepG2 cells [HepG2 (−) group] were incubated with 2 μM cholineyl-lysyl-fluorescein (CLF) with or without 250 μM benzbromarone (BEN),[32] a known inhibitor of MRP2, for 2 h and the fluorescence intensity of the "artificial bile" was measured at 485/520 (ex/em) using a microplate reader.

Cell viability assay and hepatotoxicity assessment

The viability of cells was detected by a LIVE/DEAD Viability/Cytotoxicity Kit (Thermo Fisher) according to the manufacturer's protocol. We compared the hepatotoxicity of three clinical acute hepatotoxic drugs (acetaminophen [APAP], RIF, and amiodarone [AMI]) tested by the 96-well plate model and the LSOC device. Generally, the LSOC device was perfused with the "artificial blood" containing different concentrations of APAP, RIF, and AMI for 24 h, and cell viability was determined by viable staining. For the 96-well plate model, HepG2 cells were wrapped in the same concentration of BME of the LSOC device before cultured with different concentrations of APAP, RIF, and AMI, and cell viability was also determined by viable staining.

Drug-drug interaction detection

After successful operation of the device, three drugs (50 μM RIF, 50 μM OME, 25 μM CPFX) were added to the "artificial blood" and perfused for 24 h. Then, the "artificial blood" containing 20 mM APAP was perfused for another 24 h before it was collected. The amount of Lactate dehydrogenase (LDH) in the "artificial blood" was measured using the CytoTox 96® Non-Radioactive Cytotoxicity Assay Kit (G1760, Promega, Wisconsin, USA), according to the protocol.

Imaging and data analysis

Fluorescence images were obtained using a fluorescent inverted microscope (Olympus, IX71) equipped with a mercury lamp (Olympus, U-RFLT50) and a confocal laser-scanning microscope (Olympus, FV1000). All primary antibodies (Mrp2, CD14, Ve-cadherin, F-actin, and CYP 3A/43) and secondary antibodies were purchased from Abcam, DAPI were from Sigma, and cell trackers from Invitrogen. Image processing and statistical data analysis were processed by using ImageJ (National Institutes of Health, Bethesda, MD) and SPSS 18.0 software (IBM Corp., Armonk, NY, USA), respectively. The experimental results, including error bars in graphs, represent the mean ± standard deviation (SD). One-way analysis of variance was used for statistical comparisons in the experiment, followed by a *t*-test. Statistical significance was defined as $P < 0.05$.

RESULTS AND DISCUSSIONS

Design of the liver sinusoid device

As shown in the left of Fig. 1(a), the hepatic lobe is the basic structural and functional unit of the liver and consists of a series of outwardly diverging neatly arranged liver plates. The hepatic sinusoid is a micro gap between two plates of the liver and is highly organized and performs many functions. It contains HCs and LSECs that are separated by the hepatic sinusoidal space, and hepatic stellate cells and extracellular matrix fill the gaps between HCs and LSECs. KCs are detached in the lumen of blood vessels. The vertices of HCs fuse with each other to form bile canaliculi. The major challenge for the *in vitro* liver models for preclinical drug testing is the maintenance of their typical morphological characteristics and functions like *in vivo*. To date,

three-dimensional culturing of hepatocytes, co-culturing with nonparenchymal cells, introducing fluid flow, and patterning hepatocytes in an ordered spatial arrangement have been used to preserve liver properties *in vitro* to improve the detection accuracy of drug metabolism and toxicity. For example, Revzin *et al.* co-cultured rat HCs and LX-2 cells within two parallel channels connected in the middle.[33,34] This device realized the cellular interaction between hepatocytes and stellate cells; however, this device ignores the important role of endothelial cells and Kupffer cells in the liver. Vernetti *et al.* co-cultured primary human hepatocytes with EAhy926, U937, and LX-2 cells in physiological ratios.[35] However, this device ignored the spatial arrangement of each functional cells that Kupffer cells are located on the wall of endothelial cells and stellate cells and hepatocytes inward successively. The same problem also exists in the products of companies such as Mimetas.[36,37]

As shown in the right of Figs. 1(a) and 1(b), the device contains two PMMA substrates and three PDMS layers. The chamber formed after assembly is divided into three chambers by two PC porous membranes with a diameter of 6 mm and a pore size of 1 μm. The upper and lower surfaces of the upper porous membrane were coated with EAhy926 and LX-2 cells to simulate the endothelial cell barrier. EAhy926 cells were cultured for 2 days to preferentially form a tightly connected monolayer biofilter structure. HepG2 cells were encapsulated in the BME gel and seeded in the middle chamber. HepG2 and EAhy926 cells were separated by a porous membrane, which mimicked the structure of the sinusoidal space *in vivo* where HSCs were inoculated. U937 cells were injected into the upper chamber after completion of the chip assembly. Various factors released by U937 cells pass through the EAhy926 cells layer to act on HepG2 and LX-2 cells. The real chip is shown in Fig. 1(c). This highly integrated spatial structure contains key factors of the hepatic sinusoid microenvironment. The composition, proportion, and spatial arrangement of cells mimic the features of a physiological sinusoid *in vivo*, especially two parallel channels for liver blood flow and biliary efflux with flows in the opposite direction, which may resolve the potential cholestasis problem of other liver tissues-on-a-chip reported previously.

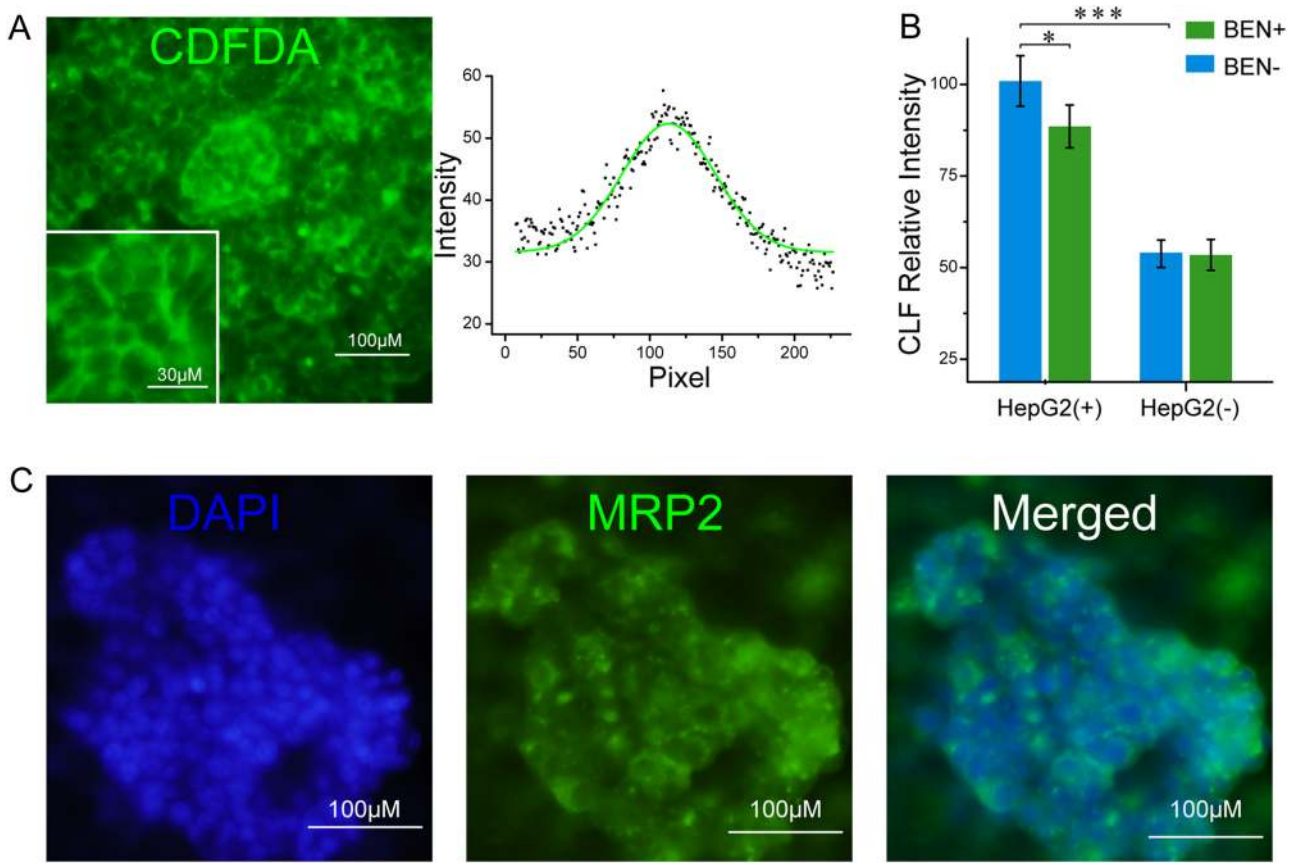

FIG. 2. Polarization of HepG2 and the formation of bile canaliculi. (a) CDFDA staining: fluorescence intensity tends to converge to the junction of HepG2 cells. The curves on the right indicate the fluorescence intensity in the gap between cells. (b) CLF quantitative experiment: the fluorescence intensity of the complete model [HepG2 (+) group] was significantly higher than the model without HepG2 cells [HepG2 (–) group], and the addition of 250 μM benzbromarone resulted in a significant decrease of fluorescence intensity. (c) Multidrug resistance protein (MRP2) staining: MRP2 (green) and DAPI (blue).

Mimicking the 3D microenvironment of liver sinusoid on a chip

To date, several structurally and functionally biomimetic *in vitro* liver models have been established to study liver biology and function, drug-induced hepatotoxicity, and liver diseases.[21,38,39] Here, we developed a novel LSOC model to mimic the complex microenvironment in the liver sinusoid for hepatotoxicity assessment based on a reported perfusion liver system using a porous permeable membrane,[40] as shown in Fig. 1, and made the following improvements. Firstly, we employed a high-density (10^7 ml^{-1}) 3D culture condition for HepG2 cells in the device, which enables the polarization of hepatocytes and forms the bile canaliculi. As shown in Fig. 2, CDFDA staining results showed that the fluorescence intensity tends to converge to the junction of HepG2 cells, indicating that CDFDA was metabolized by intracellular esterases and transported to the apex of HepG2 cells to form a canaliculus-like structure, indicating the polarization of HepG2 cells. Furthermore, we examined the tissue architecture and function of the BME-encapsulated 3D HepG2 cells in the middle chamber using H&E, live/death, and CYP fluorescent staining (Fig. S2 in the supplementary material), and the results also confirmed the polarized status of 3D HepG2 cells. Secondly, an artificial bile flow channel was fabricated in the device [Fig. 1(b)] mimicking the bile flow in the liver. The active transportation (came from blood and secreted into bile) of drugs in the liver is closely related to the hepatotoxicity of a drug or drug combinations; however, almost all liver models reported previously ignored this phenomenon and led to a biased evaluation of hepatotoxicity. In order to observe the active transportation of HepG2 cells in the liver chip, fluorescent CLF, a bile acid analogue, was added into the "artificial blood flow" indicated

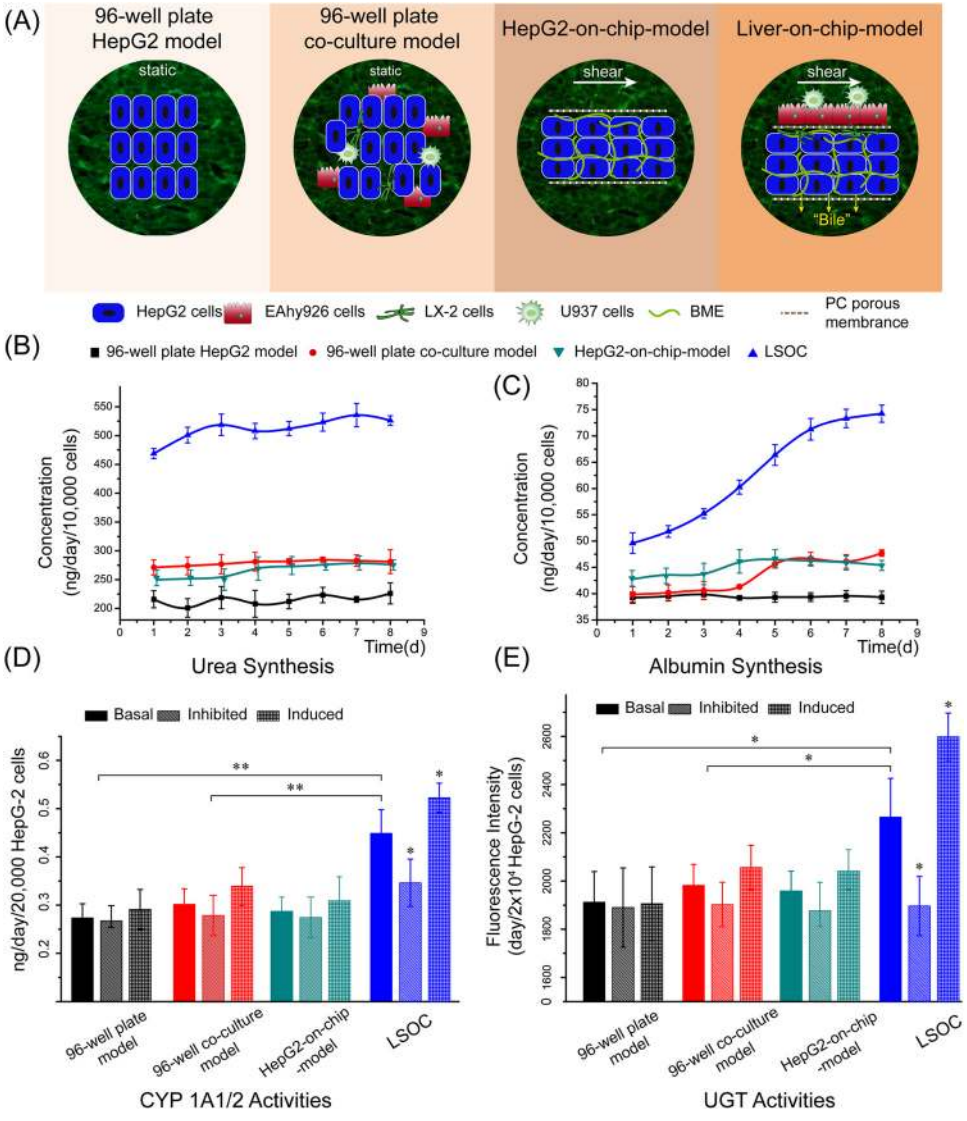

FIG. 3. The synthesis and metabolism of liver function in LSOC. (a) Four experimental models were established, model I: 96-well plate HepG2 model (HepG2 cells only), model II: 96-well plate co-culture model (four types of hepatic cell lines cultured in a mixed way), model III: HepG2-on-chip model (HepG2 cells only on chip with perfusion), model IV: LSOC device (including EAhy926 cells, HepG2 cells, LX-2 cells U937 cells with perfusion). (b) and (c) Comparison of urea production and albumin synthesis within 8 days of the four models. (d) Comparison of the basic CYP 1A1/2 metabolic activity, and the sensitivity of the four models under the effect of inducer (50 μM OME) and inhibitor (25 μM CPFX). (e) Comparison of the basic UGT metabolic activity of the four models, and the sensitivity under the effect of inducer (50 μM RIF) and inhibitor (150 μM PBD).

in Fig. 1(b), and then the CLF content was measured in the "artificial bile flow." The results [Fig. 2(b)] showed that the fluorescence intensity of the HepG2 (+) group was significantly higher than that of the HepG2 (−) group, and the addition of 250 μM benzbromarone resulted in a significant decrease of fluorescence intensity, indicating that CLF was actively transported by HepG2 cells to the "artificial bile flow." Furthermore, the staining results of the MRP2 protein, a marker of bile secretion [Fig. 2(c)],[41] also indicated the polarization and active transportation of HepG2 cells occurring in the liver chip. Thirdly, tightly connected EAhy926 cell layers (Figs. S3 and S4 in the supplementary material) were formed in the liver chip, as similar to *in vivo*, working as a barrier to avoid the direct exposure of HepG2 parenchyma to shear stress while allowing mostly "blood-borne" compounds (toxicants, nutrients, proteins, and cytokines released by U937 cells) to enter the HepG2 parenchyma. This structure reproduced the spatial relationship between blood flow and hepatocytes and the way of drugs entering hepatocyte plates that pass through endothelial cells before acting on hepatocytes. Fourthly, in the device, all types of cells express their own special markers (Fig. S3 in the supplementary material) and the proportion of HepG2 cells, LX-2 cells, EAhy926 cells, and U937 cells was consistent with that *in vivo*. Prior to assembly, approximately 2×10^5 HepG2 cells, 6×10^4 EAhy926 cells, 5×10^4 U937 cells, and 3×10^4 LX-2 cells were seeded into the chip (Table 1 in the supplementary material). Collectively, this highly organized multicellular dual-channel device made it possible to improve sensitivity and accuracy for hepatotoxicity testing.

Reproduction of the synthesis and metabolism of liver function in LSOC

In this study, BME-encapsulated HepG2 cells were used for the assembly of the hepatocyte parenchyma. We compared the HepG2 cells in our LSOC device with that in the 96-well plate HepG2 model (only HepG2 cells statically), the 96-well plate co-culture model (HepG2 cells co-culture with the other three cell lines in a mixed way statically), and the HepG2-on-chip model (only HepG2 cells perfused in the device) in the aspects of urea secretion, albumin synthesis, CYP-1A1/2 activity, and UGT activity. As shown in Figs. 3(b) and 3(c), the excretion of urea and the synthesis of albumin were higher in the liver chip compared with the other three models, reached 500 and 75 ng/day/10 000 cells at day 8, respectively. It was indicated that the biomimetic microenvironments in the liver chip were capable of enhancing the phenotypes of liver function of HepG2 cells. As can be seen in Figs. 3(b) and 3(c), urea secretion remained at a high level throughout the experiment, and the synthesis of albumin reached a high level after a steady increase. The activities of CYP-1A1/2 and UGT represented the phase I and phase II metabolic capacities of HepG2 cells, respectively. The results [Fig. 3(d), CYP-1A1/2, and Fig. 3(e), UGT] indicated that both metabolic capacities of CYP-1A1/2 and UGT of HepG2 cells in the LSOC device were superior to that in the other three models. Besides, exogenous substances also have an effect on enzyme activity. These effects of exogenous substances on metabolic enzyme activity further influence the accuracy of drug toxicity testing. As shown in Fig. 3(d), the basal activity of CYP 1A1/2 enzyme in the LSOC device was highest in all the four models. Interestingly, both inducer OME and inhibitor CPFX made no differences on the activity of CYP 1A1/2 enzyme in any of the other three models. However, there was a significant change in enzyme activity in the LSOC model. A similar phenomenon of UGT activity is shown in Fig. 3(e). These results indicated a sharper response and a greater range of activity in the LSOC device compared with the 96-well plate HepG2 model, the 96-well plate co-culture model, and the HepG2-on-chip model. This sensitivity of metabolic enzyme affected by exogenous substances contributes to the detection of potential drug interactions. To prove further the influence of shear stress for better liver function, we compared the urea secretion, albumin synthesis, CYP-1A1/2 activity, and UGT activity of the LSOC device to that without perfusion while the

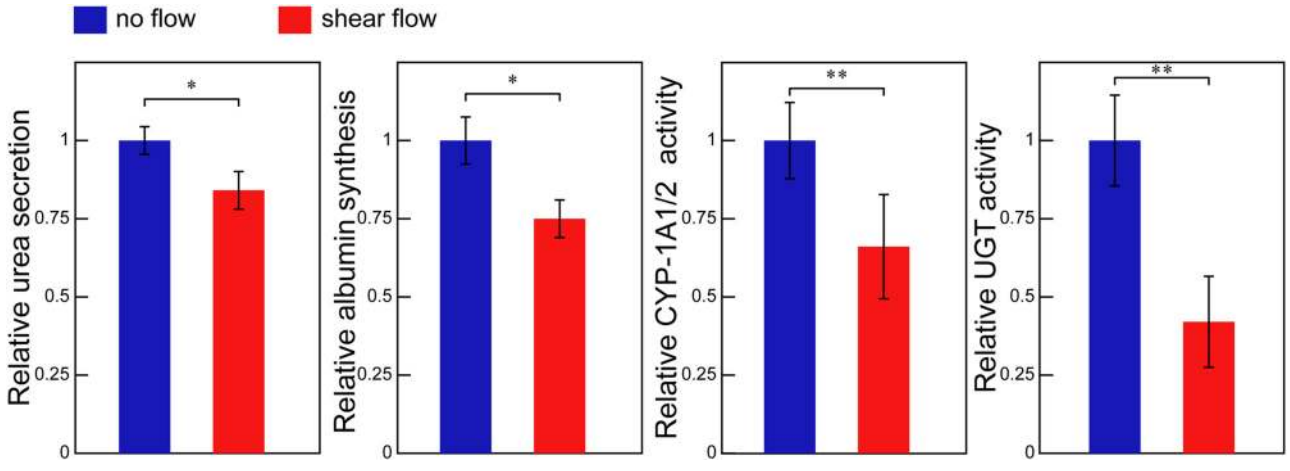

FIG. 4. Functional tests of liver-specific secretion and metabolism (urea secretion, albumin synthesis, CYP-1A1/2, and UGT activities) with (blue) or without (red) shear flow in LSOC device.

medium exchange every day; results at day 4 (Fig. 4) show that urea, albumin, CYP-1A1/2, and UGT are higher than that without perfusion, indicating that shear force helps to improve liver function of synthesis and metabolism *in vitro*. Thus, this LSOC device can be used for guiding the clinical principles of drug combination, particularly when the drug-drug combination occurred.

Increasing sensitivity of hepatotoxicity testing of HepG2 cells in the LSOC device

The low accuracy of HepG2 cell based *in vitro* models for drug evaluation limits its application. Here, we verified the ability of the LSOC device to detect liver toxicity, which was induced by three clinical acute hepatotoxic drugs [APAP, RIF, and amiodarone (AMI)]. In experiments, APAP was perfused in the "artificial blood" at concentrations of 5, 15, and 25 mM for 24 h, and cell viability was determined by viable staining as shown in Figs. 5(a) and 5(b). As the APAP concentration increased, the cell mortality rate went up gradually. In addition, after exposure to the same concentration (5, 15, and 25 mM) of APAP, the mortality rate of HepG2 cells in the chip model (39%, 54%, and 87%) was higher than that in the 96-well plate HepG2 model (18%, 27%, and 42%), presumably because of the higher drug metabolism ability, more consistent oxygen content of the media, cross talk between multiple cell types, the impact from shear stress, and the rapid removal of cellular by-products in the chip. The release of biochemical markers (LDH, AKP, AST, and ALT) in the "artificial blood" also showed the same trend as mortality rate (Fig. S5 in the supplementary material). Furthermore, after exposure to APAP, RIF, and AMI for 24 h, we plotted the dose-related toxicity curves and calculated the TC50 as 9.8 mM,

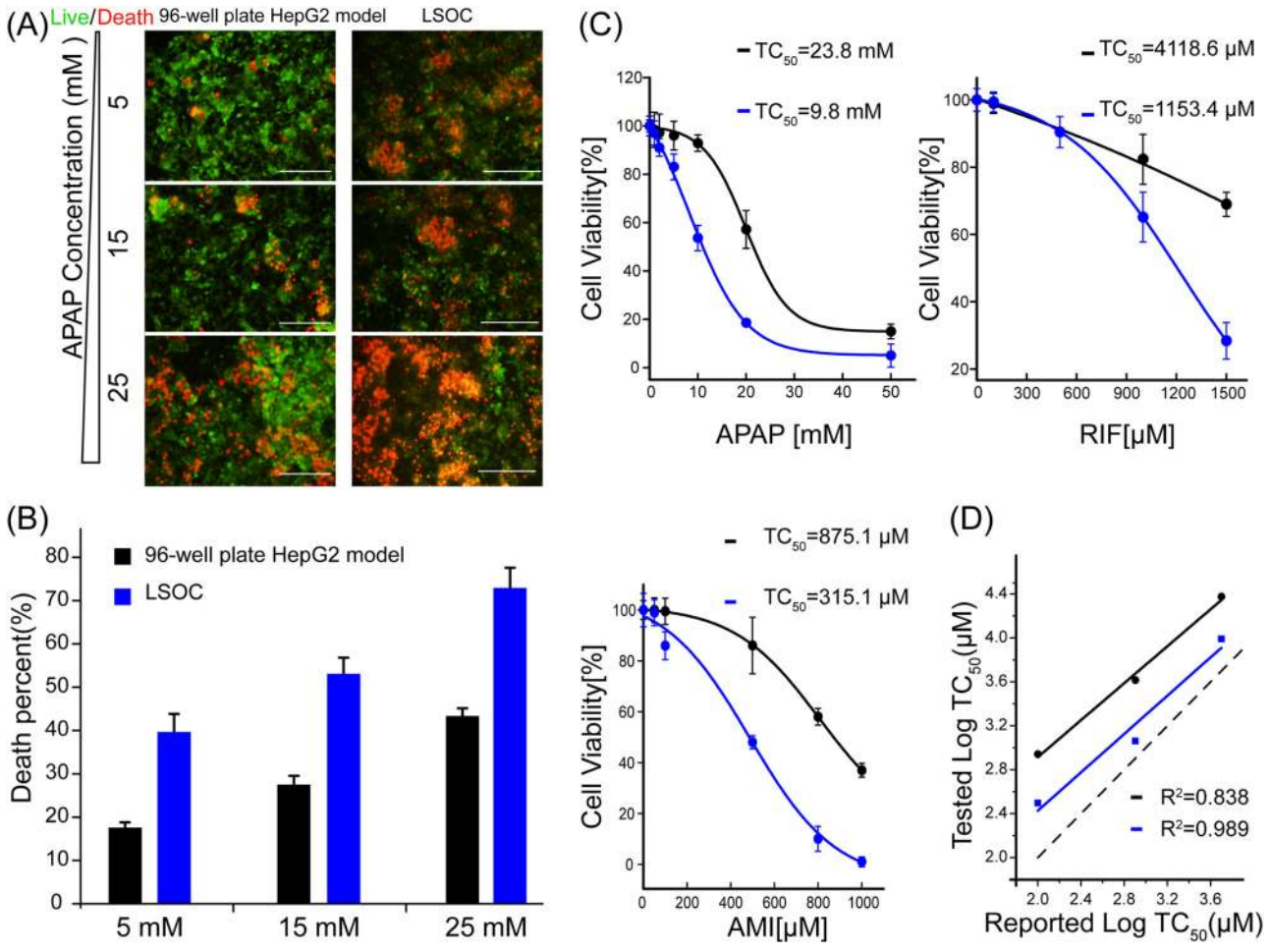

FIG. 5. Comparison of drug hepatotoxicity testing results in the 96-well plate HepG2 model and LSOC device. (a) Comparison of cell viability in the two models induced by 5 mM, 15 mM, and 25 mM APAP (green represents live, red represents death); (b) Statistical analysis of (A); (c) Dose-related toxicity curves of APAP, RIF, and AMI. (d) IVIVC comparison of TC50 values tested by primary human hepatocytes to that by the LSOC device, showing a better fit of the chip model at 45° (dotted lines), indicating a higher correlation *in vivo*. Scare bar = 200 μm.

1153.4 μM, and 315.1 μM [Fig. 5(c)], respectively. We compared the TC50 of primary human hepatocytes of the three drugs reported in the literature (APAP: 5 mM, RIF: 1400 μM, AMI: 100 μM);[42,43] the *in vitro–in vivo* correlation (IVIVC) result comparing TC50 values of primary human hepatocytes to our device[44] showed that results from the chip model were closer to the 45° diagonal (dotted line) with an $R^2 = 0.989$, which indicated a higher accuracy of hepatotoxicity testing than that by 96-well plate HepG2 model [Fig. 5(d)].

Testing drug-drug interaction using cell lines derived LSOC device

Drug-drug interaction is another focus of drug development and clinical application. Many drugs affect the activity of drug-metabolizing enzymes thus lead to reducing or increasing toxicity of other drugs when used in combination. Thus, the ability to predict accurate drug-drug interactions is another requisite ability for *in vitro* liver models. In this experiment, we compared the hepatotoxicity of APAP in combination with three drugs that have been shown to influence the metabolism activity of phase I or phase II. As a result [Fig. 6(a)], when 50 μM RIF or 25 μM CPFX was used in combination with APAP, the release of LDH in the "artificial blood" was significantly reduced, indicating that this combination reduced the toxicity of APAP. This result was entirely consistent with increased metabolism of acetaminophen through an alternate oxidative metabolism isoenzyme. In contrast, when APAP combined with 50 μM OME, the release of LDH in the "artificial blood" increased significantly, indicating that this combination increased the toxicity of APAP. Notably, this phenomenon was not found in the 96-well plate HepG2 model. To further confirm the ability to detect drug interactions of the device, we compared the variation of hepatotoxicity of the combinations in the device to the classical primary hepatocyte plate model, as primary hepatocytes are considered the gold standard.[7,45] The results [Fig. 6(b)] showed that variations of hepatotoxicity in the liver chip were −17.15%, 14.88%, and −19.74%, while these data obtained from traditional primary hepatocytes plate model were −13.22%, 13.51%, and −15.81%. It suggested that results tested by the LSOC device were equivalent to that by primary hepatocytes, which further confirmed the practicality of the LSOC device for the study of potential drug-drug interactions. The reasons for these results might be that this multi-cell perfusion LSOC device creates a microenvironment that is similar *in vivo*. For example, the enriched nutrition and sufficient oxygen supply allow cells to maintain a stable state and increase paracrine signaling between cells. The intercellular communication between HepG2 cells and the three other cell lines enhanced APAP induced hepatotoxicity and regulated the activity of metabolic enzymes of HepG2 cells.

Collectively, this device has significant advantages that made it possible to reflect drug-drug interactions and increase the accuracy of hepatotoxicity testing using HepG2 cells. Thus, this proposed liver device provides an alternative approach for the assessment of hepatotoxicity and potential drug-drug interactions.

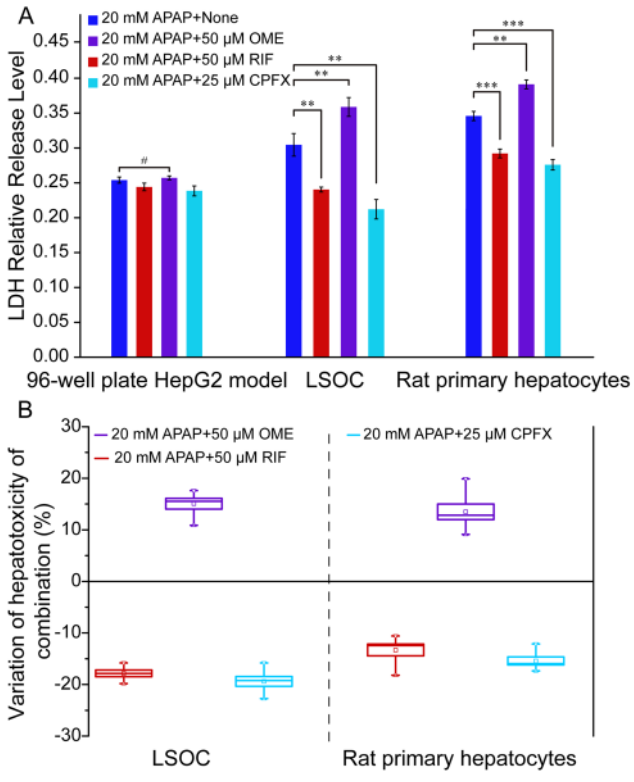

FIG. 6. Comparison of drug interactions tested by the three experimental models. (a) Fluctuation of hepatotoxicity (LDH release) of 20 mM APAP in combination with 50 μM RIF, 50 μM OME, and 25 μM CPFX tested by the 96-well plate HepG2 model, LSOC device, and rat primary hepatocytes on the plate. (b) Variation of hepatotoxicity of acetaminophen-based drug-drug interaction tested by the LSOC device and that by rat primary hepatocytes.

CONCLUSIONS

In conclusion, we propose a LSOC device for hepatotoxicity evaluation, as well as drug-drug interactions. The proportion and the spatial structure of the four types of hepatic cells were integrated in an orderly manner, which simulated the complex structure and microenvironment of hepatic sinusoids *in vivo*, while maintaining liver functions. Our results showed that the LSOC device improved the accuracy of hepatotoxicity testing and made it possible to detect potential drug-drug interaction using HepG2 cells. Thus, we believe that the cell lines derived liver model could serve as an alternative platform for testing drug-induced hepatotoxicity, as well as liver function and disease.

SUPPLEMENTARY MATERIAL

See the supplementary material for standard curves of absorbance of urea, albumin and cell number (Fig. S1), H&E, live/death and CYP 3A43 staining of 3D HepG2 cells in the middle chamber (Fig. S2), identification of four types of hepatic cell lines on chip after cultured for 48 h (Fig. S3), apparent permeability of EAhy926 cell-layer (Fig. S4), and release of biochemical markers in the "artificial blood" after exposed to different concentration of APAP (Fig. S5).

ACKNOWLEDGMENTS

This work was supported by the National Natural Science Foundation of China (NNSFC) (No. 21675017), the National Key Research and Development Program of China (No. 2017YFC1702001), and Sanming Project of Medicine in Shenzhen (No. SZSM201612049)

REFERENCES

[1]L. A. Vernetti, A. Vogt, A. Gough, and D. L. Taylor, Clinics in Liver Disease **21**, 197 (2017).
[2]W. Zhang, L. Chen, H. Feng, W. Wang, Y. Cai, F. Qi, X. Tao, J. Liu, Y. Shen, X. Ren, X. Chen, J. Xu, and Y. Shen, Free Radic. Biol. Med. **112**, 24 (2017).
[3]S. J. Kwon, D. W. Lee, D. A. Shah, B. Ku, S. Y. Jeon, K. Solanki, J. D. Ryan, D. S. Clark, J. S. Dordick, and M. Lee, Nat. Commun. **5**, 3739 (2014).
[4]K. Yu, S. Nadanaciva, P. Rana, D. W. Lee, B. Ku, A. D. Roth, J. S. Dordick, Y. Will, and M. Lee, Arch. Toxicol. **92**(3), 1295–1310 (2017).
[5]Y. Zhuo, J. Wu, X. Yan, M. Guo, N. Liu, H. Zhou, L. Liu, and N. Li, Anal. Chem. **89**, 13167 (2017).
[6]Y. Weng, S. Chang, M. Shih, S. Tseng, and C. Lai, Adv. Mat. **29**, 1701545 (2017).
[7]R. L. Sison-Young, V. M. Lauschke, E. Johann, E. Alexandre, S. Antherieu, H. Aerts, H. H. J. Gerets, G. Labbe, D. Hoët, M. Dorau, C. A. Schofield, C. A. Lovatt, J. C. Holder, S. H. Stahl, L. Richert, N. R. Kitteringham, R. P. Jones, M. Elmasry, R. J. Weaver, P. G. Hewitt, M. Ingelman-Sundberg, C. E. Goldring, and B. K. Park, Arch. Toxicol. **91**, 1385 (2017).
[8]Y. Liu, H. Li, S. Yan, J. Wei, and X. Li, Biomacromolecules **15**, 1044 (2014).
[9]N. I. Kalinina, V. Y. Sysoeva, K. A. Rubina, Y. V. Parfenova, and V. A. Tkachuk, Acta Naturae **3**(4), 30–37 (2011).
[10]F. Zheng, F. Fu, Y. Cheng, C. Wang, Y. Zhao, and Z. Gu, Small **12**, 2253 (2016).
[11]J. Deng, Y. Qu, T. Liu, B. Jing, X. Zhang, Z. Chen, Y. Luo, W. Zhao, Y. Lu, and B. Lin, Microphysiol. Syst. **2**, 8 (2018).
[12]T. Osaki, V. Sivathanu, and R. D. Kamm, Curr. Opin. Biotechnol. **52**, 116 (2018).
[13]Y. Qu, F. An, Y. Luo, Y. Lu, T. Liu, W. Zhao, and B. Lin, Biomaterials **155**, 41 (2018).
[14]X. Yang, K. Li, X. Zhang, C. Liu, B. Guo, W. Wen, and X. Gao, Lab Chip **18**(3), 486–495 (2018).
[15]Y. Wang, L. Wang, Y. Zhu, and J. Qin, Lab Chip **18**(6), 851–860 (2018).
[16]J. U. Lind, M. Yadid, I. Perkins, B. B. O'Connor, F. Eweje, C. O. Chantre, M. A. Hemphill, H. Yuan, P. H. Campbell, J. J. Vlassak, and K. K. Parker, Lab Chip **17**(21), 3692–3703 (2017).
[17]N. Mori, Y. Morimoto, and S. Takeuchi, Biomaterials **116**, 48 (2017).
[18]D. F. G. Hendriks, L. Fredriksson Puigvert, S. Messner, W. Mortiz, and M. Ingelman-Sundberg, Sci. Rep. **6**, 35435 (2016).
[19]F. Yu, R. Deng, W. Hao Tong, L. Huan, N. Chan Way, A. IslamBadhan, C. Iliescu, and H. Yu, Sci. Rep. **7**, 14528 (2017).
[20]K. Rennert, S. Steinborn, M. Gröger, B. Ungerböck, A. Jank, J. Ehgartner, S. Nietzsche, J. Dinger, M. Kiehntopf, H. Funke, F. T. Peters, A. Lupp, C. Gärtner, T. Mayr, M. Bauer, O. Huber, and A. S. Mosig, Biomaterials **71**, 119 (2015).
[21]X. Li, S. M. George, L. Vernetti, A. H. Gough, and D. L. Taylor, Lab Chip **18**, 2614 (2018).
[22]Y. Toh, T. C. Lim, D. Tai, G. Xiao, D. van Noort, and H. Yu, Lab Chip **9**, 2026 (2009).
[23]Y. B. A. Kang, T. R. Sodunke, J. Lamontagne, J. Cirillo, C. Rajiv, M. J. Bouchard, and M. Noh, Biotechnol. Bioeng. **112**, 2571 (2015).
[24]H. M. M. Ahmed, S. Salerno, S. Morelli, L. Giorno, and L. De Bartolo, Biofabrication **9**(2), 025022 (2017).
[25]S. Lee, D. Y. No, E. Kang, J. Ju, D. Kim, and S. Lee, Lab Chip **13**, 3529 (2013).
[26]M. Jang, P. Neuzil, T. Volk, A. Manz, and A. Kleber, Biomicrofluidics **9**(3), 034113 (2015).
[27]H. S. Kruitwagen, L. A. Oosterhoff, I. G. W. H. Vernooij, I. M. Schrall, M. E. van Wolferen, F. Bannink, C. Roesch, L. van Uden, M. R. Molenaar, J. B. Helms, G. C. M. Grinwis, M. M. A. Verstegen, L. J. W. van der Laan, M. Huch, N. Geijsen, R. G. Vries, H. Clevers, J. Rothuizen, B. A. Schotanus, L. C. Penning, and B. Spee, Stem Cell Rep. **8**, 822 (2017).
[28]M. B. Esch, G. J. Mahler, T. Stokor, and M. L. Shuler, Lab Chip **14**, 3081 (2014).
[29]P. Godoy, N. J. Hewitt, U. Albrecht, M. E. Andersen, N. Ansari, S. Bhattacharya, J. G. Bode, J. Bolleyn, C. Borner, J. Böttger, A. Braeuning, R. A. Budinsky, B. Burkhardt, N. R. Cameron, G. Camussi, C. Cho, Y. Choi, J. Craig Rowlands, U. Dahmen, G. Damm, O. Dirsch, M. T. Donato, J. Dong, S. Dooley, D. Drasdo, R. Eakins, K. S. Ferreira, V. Fonsato, J. Fraczek, R. Gebhardt, A. Gibson, M. Glanemann, C. E. P. Goldring, M. J. Gómez-Lechón, G. M. M. Groothuis, L. Gustavsson, C. Guyot, D. Hallifax, S. Hammad, A. Hayward, D. Häussinger, C. Hellerbrand, P. Hewitt, S. Hoehme, H. Holzhütter, J. B. Houston, J. Hrach, K. Ito, H. Jaeschke, V. Keitel *et al.*, Arch. Toxicol. **87**, 1315 (2013).
[30]L. Prodanov, R. Jindal, S. S. Bale, M. Hegde, W. J. McCarty, I. Golberg, A. Bhushan, M. L. Yarmush, and O. B. Usta, Biotechnol. Bioeng. **113**, 241 (2016).
[31]J. S. Passmore, P. T. Lukey, and S. R. Ress, Immunology **102**, 146 (2001).
[32]L. Saab, J. Peluso, C. D. Muller, and G. Ubeaud Sequier, Cytometry Part A **83A**, 403 (2013).
[33]Q. Zhou, D. Patel, T. Kwa, A. Haque, Z. Matharu, G. Stybayeva, Y. Gao, A. M. Diehl, and A. Revzin, Lab Chip **15**, 4467 (2015).
[34]A. Haque, P. Gheibi, G. Stybayeva, Y. Gao, N. Torok, and A. Revzin, Sci. Rep. **6**, 36077 (2016).
[35]L. A. Vernetti, N. Senutovitch, R. Boltz, R. DeBiasio, T. Y. Shun, A. Gough, and D. L. Taylor, Exp. Biol. Med. **241**, 101 (2016).
[36]S. J. Trietsch, G. D. Israëls, J. Joore, T. Hankemeier, and P. Vulto, Lab Chip **13**, 3548 (2013).
[37]A. Junaid, A. Mashaghi, T. Hankemeier, and P. Vulto, Curr. Opin. Biomed. Eng. **1**, 15 (2017).
[38]A. M. Ortega-Prieto, J. K. Skelton, S. N. Wai, E. Large, M. Lussignol, G. Vizcay-Barrena, D. Hughes, R. A. Fleck, M. Thursz, M. T. Catanese, and M. Dorner, Nat. Commun. **9**, 682 (2018).
[39]T. Kostrzewski, T. Cornforth, S. A. Snow, L. Ouro-Gnao, C. Rowe, E. M. Large, and D. J. Hughes, World J. Gastroenterol. **23**, 204 (2017).
[40]Y. Du, N. Li, H. Yang, C. Luo, Y. Gong, C. Tong, Y. Gao, S. Lu, and M. Long, Lab Chip **17**, 782 (2017).
[41]M. Depreter, T. Walker, K. De Smet, S. Beken, I. Kerckaert, V. Rogiers, and F. Roels, Histochem. J. **34**, 139 (2002).
[42]S. Prill, D. Bavli, G. Levy, E. Ezra, E. Schmälzlin, M. S. Jaeger, M. Schwarz, C. Duschl, M. Cohen, and Y. Nahmias, Arch. Toxicol. **90**, 1181 (2016).
[43]S. R. Khetani and S. N. Bhatia, Nat. Biotechnol. **26**, 120 (2008).
[44]D. Bavli, S. Prill, E. Ezra, G. Levy, M. Cohen, M. Vinken, J. Vanfleteren, M. Jaeger, and Y. Nahmias, Proc. Natl. Acad. Sci. U.S.A. **113**, E2231 (2016).
[45]J. A. Kyffin, P. Sharma, J. Leedale, H. E. Colley, C. Murdoch, P. Mistry, and S. D. Webb, Toxicol. In Vitro **48**, 262 (2018).